RSC Advances

Synthesis of ZnAl2O4:(Er3+,Yb3+) spinel-type nanocrystalline upconverting luminescent marker in HeLa carcinoma cells , using a combustion aerosol method route

Journal:	*RSC Advances*
Manuscript ID:	RA-ART-09-2014-010976
Article Type:	Paper
Date Submitted by the Author:	22-Sep-2014

Complete List of Authors:	Kaminska, Izabela; Institute of Physics Polish Academy of Science, Laboratory of Biological Physics Fronc, Krzysztof; Institute of Physics Polish Academy of Science, Laboratory of Biological Physics Sikora, Bozena; Institute of Physics Polish Academy of Science, Laboratory of Biological Physics Koper, Kamil; Institute of Biochemistry and Biophysics PAS, ul. Pawińskiego 5a, 02- 106, ; Institute of Genetics and Biotechnology, Faculty of Biology, University of Warsaw, ul. Pawinskiego 5a, 02-106, Minikayev, Roman; Institute of Physics Polish Academy of Science, Paszkowicz, Wojciech; Institute of Physics Polish Academy of Science, Sobczak, Kamil; Institute of Physics Polish Academy of Science, Wojciechowski, Tomasz; Institute of Physics Polish Academy of Science, Chwastyk, Mateusz; Institute of Physics Polish Academy of Science, Reszka, Anna; Institute of Physics Polish Academy of Science, Kowalski, Bogdan; Institute of Physics Polish Academy of Science, Stępień, Piotr; Institute of Biochemistry and Biophysics PAS, ul. Pawińskiego 5a, 02- 106, ; Institute of Genetics and Biotechnology, Faculty of Biology, University of Warsaw, ul. Pawinskiego 5a, 02-106, Elbaum, Danek; Institute of Physics Polish Academy of Science,

Cite this: DOI: 10.1039/c0xx00000x

www.rsc.org/xxxxxx

Synthesis of $ZnAl_2O_4$:(Er^{3+},Yb^{3+}) spinel-type nanocrystalline upconverting luminescent marker in HeLa carcinoma cells , using a combustion aerosol method route

Izabela Kamińska[a,*], Krzysztof Fronc[a], Bożena Sikora[a], Kamil Koper[b,c], Roman Minikayev[a], Wojciech Paszkowicz[a], Kamil Sobczak[a], Tomasz Wojciechowski[a], Mateusz Chwastyk[a], Anna Reszka[a], Bogdan J. Kowalski[a], Piotr Stępień[b,c], Danek Elbaum[a]

Received (in XXX, XXX) Xth XXXXXXXXX 20XX, Accepted Xth XXXXXXXXX 20XX
DOI: 10.1039/b000000x

Efficiently upconverting, spherical $ZnAl_2O_4$ nanoparticles (NPs), doped with erbium and ytterbium, were synthesized by a combustion aerosol method (CAM) and transported to cytosol of human carcinoma cell line (HeLa) for the first time. Spherical, 82-140 nm spinels were obtained, at various concentrations of the substrates. The nanoparticles were optimized to emit in the red luminescence range (Er^{3+}, 661nm, $^4F_{9/2} \rightarrow {}^4I_{15/2}$) when excited with Near Infra Red light. Lower absorption and scattering by aqueous biological samples, compared to the green emission (Er^{3+}, 550 nm, $^2H_{11/2} \rightarrow {}^4I_{15/2}$, $^2S_{3/2} \rightarrow {}^4I_{15/2}$), was responsible for the preferred upconversion. In addition, application of the near infrared light significantly reduced cellular autofluorescence and light scattering. The X-ray diffraction, transmission electron microscopy, scanning electron microscopy and photoluminescence spectra were employed to characterize the synthesized samples. Energy dispersive X-ray microanalysis was used to confirm the composition and distribution of the nanoparticles through spectrum and elemental mapping. The hydrophilic, spherical NPs, coated with PVP (Polyvinylpyrrolidone*)*, in the presence of liposomal transfection factor - Lipofectamine, were endocytosed into living HeLa cells and followed as luminescent markers by confocal laser scanning microscopy. We present optimized protocols for the NPs synthesis and delivery of the spinels to the cancer cells for bioimaging.

1. Introduction

Significant effort has been recently devoted to synthesize an optimal biomarker capable to image diagnostically useful cellular structures. An optimal luminophore should combine several properties: *a*. relatively low toxicity, *b*. small size (compared to cell), *c*. to form separate nanoparticles with surfaces accessible to biofunctionalization, *d*. efficient emission in the region of low auto fluorescence while excited by light of relatively low absorption and light scattering. Spherical $ZnAl_2O_4$ spinels, doped with erbium and ytterbium, are promising bioimaging candidates. $ZnAl_2O_4$ (mineral gahnite) is a popular wide-band gap semiconductor (E_g = 3.8eV).[1,2]. This material is a metal aluminate of spinel structure (*Fd*-3*m* space group). It is frequently used as ceramic, electronic and catalytic material.[3,4,5,6] It has a combination of several robust properties: high melting temperature, high strength, and high resistance to chemical attack. [3, 7] The Zn site exhibits tetrahedral coordination with the T_d site symmetry. The Al site has a sixfold distorted octahedral coordination related to the D_{3d} point group.[7, 8] Combined with rare earth ions such as erbium Er^{3+} and ytterbium Yb^{3+} the spinels show interesting luminescent properties. Yb^{3+} ions, in this crystal, absorb light in a band between 940 nm and 1µm, next this excitation is transfered to erbium. Yb ion can be readily excited by a commercially available diode lasers.[9] This cation is an excellent sensitizer for upconversion (UC). The phenomenon of upconversion, where an antistoke lower wavelength emission results from a higher wavelength excitation, can take place through four different mechanisms: *a*. excited state absorption (ESA), *b*. energy transfer upconversion (ETU), *c*. photon avalanche (PA) and *d*. energy migration - mediated upconversion (EMU). [10, 11, 12] ETU was first reported by Auzel. [13] The author proposed to consider cases where the activators were in an excited state. In addition, they argue that the activator ions, possessing several (*n*) excited states but only single ground state, can be responsible for the *n*-photons additively. This becomes apparent observing that the energy differences, not the absolute energy, can be exchanged between the ions. [13] The studied reaction involves a non-radiative energy transfers between: a sensitiser (Yb^{3+}) and an activator (Er^{3+}). The sensitizer is excited after absorption of an incident photon, then it relaxes to the ground state by transferring its energy to a neighboring activator, raising the latter to a higher-energy state. In general, the energy transfer processes are based on the electric dipole-dipole interactions. [14] Upconverting nanoparticles have been used for various biological applications: immunochromatography-detecting human chorionic gonadotropin and detecting nucleic

acid sequences [15] microarray-nucleic acid microarrays, immunoassay-detection of drugs of abuse and E. coli, [16] as well as cellular surface antigens [17] and several others. In our previous work we applied non-functionalized UC spherical nanoparticles incubated with *HeLa* cell lines and observed them to be endocytosed by the cells. [18] It is still essential to develop a new generation of nanoscale phosphors, which exhibit improved luminescence and functional properties compared to their commercially available counterparts. Several groups have synthesized $ZnAl_2O_4$ based materials applying different methodology. Camargo *et al.* [19] reported a synthesis of Er^{3+}/Yb^{3+} co-doped $ZnAl_2O_4$ phosphors by the combustion reaction method. The popular combustion method renders the nanoparticles highly aggregated thus unsuitable for a direct bio-applications.

We applied a combustion aerosol method, a promising nanoparticle synthesis method, because it allows us to produce separate nanoparticles and utilize a wide range of precursors for an efficient synthesis of a broad spectrum of functional nanoparticles.[20, 21] The combustion aerosol method enables to fractionate the nanoparticles to optimize their size. The heat released from the combustion of liquid fuel and the precursor itself can provide a required high-temperature environment. The temperature of furnace process and particle residence time, which are the most important parameters determining the characteristics of the particles, [20] can be easily controlled by varying fuel and oxidizer ratio. Chen *et al.* [22] prepared Eu^{3+}-doped $ZnAl_2O_4$ phosphors and obtained spherical porous $ZnAl_2O_4$:Eu^{3+} phosphors that excited at λ_{ex} = 392 nm exhibited red luminescence.

We present, to the best of our knowledge, for the first time, synthesis and biological application of spherical upconverting $ZnAl_2O_4$ co-doped Er^{3+} and Yb^{3+} spinels, obtained by a combustion aerosol method, for intracellular imagining in HeLa cells.

2. Experimental procedures

2.1 Starting materials

Spherical polydisperse $ZnAl_2O_4$:Er^{3+},Yb^{3+} (1:5) nanoparticles were prepared by a combustion aerosol method. Combustion aerosol synthesis involves mixing nitrates of metallic ions acting as oxidizing reagents with urea that acts as the reducing agent. [23] This redox mixture consisted of zinc nitrates-$Zn(NO_3)_2\times6H_2O$, Chempur), aluminum nitrate-$Al(NO_3)_3\times9H_2O$, Fluka), urea-$CO(NH_2)_2$, Aldrich, erbium nitrate-$Er(NO_3)_3\times6H_2O$, Aldrich, ytterbium nitrate-$Yb(NO_3)_3\times6H_2O$, Aldrich. The initial composition of such mixture is calculated based on the total valence number of the reacting elements, so as to favour the desired Er^{3+}/Yb^{3+} proportion, using the concepts of propellants chemistry. [24] Stoichiometric amounts of the reductors and oxidants were thoroughly mixed in minimum amount of water. The stated molar concentrations and suitable composition are summarized in Table 1.

2.2 Combustion aerosol method for producing spinel $ZnAl_2O_4$: Er^{3+}, Yb^{3+} nanoparticles

In order to increase the reaction temperatures, ethanol was added to the solution. The transparent solution was put into a 80 ml vessel and connected to the a nozzle inhaler F400 CONDOR II a portable device equipped with a pneumatic gas compressor Fig. 1a. The apparatus was driven on a continuous basis. It cooperated with a nebulizer powered by a compressed gas. The flow of the compressed gas through nozzles of the nebulizer having a diameter of a fraction of a millimeter, produced a sudden depressurization of the under pressured gas which was sucked into an aqueous reaction solution in the region of the nozzle nebulizer. In the nozzle the liquid was entrained by the stream of the high velocity gas and generated small droplets. Fig. 1b shows the schematic of a high - temperature combustion aerosol process for the production of nanoscale ceramic powders and pictures of the actual system. Stages of the nanoparticles formation are shown in Fig. 1c. The aerosol precursors produced by the nebulizer consisted of droplets roughly 4 μm in diameter, which were injected into a high temperature area of the furnace at the temperature of 1100 ^oC, later followed by the ignition and evaporation of the solvents. Subsequently they broke up into many smaller droplets. Driven by kinetic energy the particles collided with each other to form clusters, later colliding with other molecules and each other to form larger, more stable aggregates, a process called collision growth. When the sintering time is greater than the characteristic time of particle collisions, conglomerates can be created. [25, 26] In the next step the obtained powder was collected from the quartz tube and subsequently calcined in air at 990 ^oC for 3h in order to improve the structure and to get rid of trace reactants. Next we used (polyvinylpyrrolidone) PVP as a capping agent [27] to stop nanoparticle aggregation and to make them hydrophilic. The resulting nanopowder was suspended in 40 ml of ethanol, and the polymer in 20 ml of ethanol. Then the two substances were combined and stirred for 6 h at 45 °C. The solution was then cooled to room temperature, centrifuged at 22 °C for 15 min, at a speed of 6000 rpm and dried at 50 ^oC.

The primary advantages of the aerosol particle combustion method are: relatively small particle size, narrow size distribution and high purity of the particles produced. The proposed technique allows a large scale production of nanoparticles with the upconversion efficiency similar to the upconversion efficiency obtained by the solution combustion method. By applying the aerosol method we obtained spherical, separate nanoparticles.

Table 1. A list of all performed experiments.

Sample	Molar concentration (M)	Composition
A1	4.00	urea
A2	4.00	urea,ethanol
A3	2.70	ethanol
A4	0.10	ethanol
A5	0.02	ethanol

2.3 Cell labeling

The human carcinoma cell line (HeLa) derived from cervical cancer was used in this study. The cells were cultivated using Dulbecco modified Eagle medium (DMEM) containing 10% (vol/vol) fetal calf serum (FCS), 100 units/ml penicillin and 100 μg/ml streptomycin. Cultures of cells were incubated at 37 °C in

a humidified atmosphere containing 5% CO_2. Liposomal vesicle transfection agent (Lipofectamine 2000) was used to transport nanoparticles into the cells. Cells were cultured in 6 well plates (6 x 10 cm²) at a density of 100000/plate. Cells were incubated with the $ZnAl_2O_4:Er^{3+},Yb^{3+}$ nanoparticles with the transfection agent: in accordance with the procedure previously reported by us. [18] 10µl nanoparticles in an aqueous solution, at concentration of 10^{-3}g ml^{-1}, was dissolved in 500 µl miliR H_2O. 20 µl Lipofectamine 2000 was dissolved in 500 µl miliR H_2O and incubated for 15 minutes. Both solutions were mixed and incubated for 20 minutes. 250 µl of this solution was added to plates seeded with HeLa cells and incubated for 24 hours. The medium was removed and the cells were fixed with filtered paraformaldehyde.

2.4 Characterization and physical properties

X-ray diffraction (XRD) was used to characterize the crystallite size of the spinel phase. Nanoparticles were investigated using a Philips X´Pert Pro Alpha1 MPD diffractometer (Panalytical) (λ = 1.5406 Å). The morphology and size of the particles was examined using a scanning electron microscope (SEM). For the measurement of cathodoluminescence (CL), the nanopowder was placed on a sample holder of a scanning electron microscope (SEM). The SEM has an attachment for measuring CL with a CCD camera. Application of EDS attached to the SEM enabled us to carry out qualitative and quantitative analysis of the distribution of elements in specified surface microareas (analysis points) and specified surface analysis (mapping) in the samples. Transmission electron microscopy (TEM) a JEOL JEM2000EX operated at 200 kV was applied to examine the size and shape of prepared samples. Images recorded on film using the Nikon LS-8000 scanner were subjected to digital processing for further analysis. Observations were performed using diffraction contrast techniques: bright field-image forming of the incident beam and the dark-field-image forming with the diffracted beam. HRTEM investigations were done with the use of a Titan- Cubed 80-300 electron microscope at 300 keV beam energy. The photoluminescence spectra of the samples were measured with a Jobin Yvon-SPEX 270 M monochromator. The excitation (λ_{exc} = 965 nm) source was a IR laser diode (ThorLabs LDC 220C) with a maximum power density of 584 mW mm^{-2} (CW - continuous wave). Bioimaging of HeLa cells, incubated with $ZnAl_2O_4:Er^{3+},Yb^{3+}$, was performed on a commercial Confocal Laser Scanning Microscope (Leica TCS SP5) equipped with a multiphoton Ti:Sapphire laser (Spectra-Physics Mai Tai BB, 710-990 nm, 80 femtoseconds, 80 MHz). The samples were excited by a 980 nm wavelength laser (femtoseconds), and two visible UC emission channels were detected at green (512-587 nm) and red (627-700 nm) spectral regions. Autofluorescence of HeLa cells was observed when excited at 488 nm with an argon laser and detected at 497-541 nm.

3 Results and discussion

3.1. Structural properties

Five $ZnAl_{1.9}Er_{0.017}Yb_{0.083}O_4$ NPs samples were obtained at various precursors compositions. A list of all performed experiments is summarized in Table 1. The patterns of the $ZnAl_2O_4:Er^{3+},Yb^{3+}$ nanoparticles are shown in Fig. 2. Almost all the reflections of those materials could be indexed to those of standard $ZnAl_2O_4$. [28] In all the investigated samples, we observed the main phase resulting from the $ZnAl_2O_4$ spinel structure (*Fd*-3*m* space group). In the sample A1 annealed at 990 °C for 3 h and A2 which was not annealed we observed the ZnO phase (wurtzite) space group ($P_{63}mc$). Table S1 in Supporting Informations shows a summary of the lattice parameters, present phases, main phase size and strongest five peaks characteristic in selected samples of $ZnAl_2O_4:Er^{3+},Yb^{3+}$ spinels in the form of powder. Analysis of the diffraction patterns was performed by Rietveld [29, 30] applying FULLPROF program, which was implemented in the software package WinPLOTR. [31]

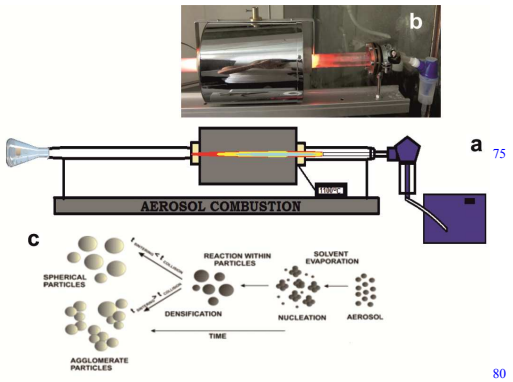

Fig. 1 Schematic of a high-temperature combustion aerosol process for the production of nanoscale ceramic powders. a, Pictures of the real setup. b, Stages of the formation of nanoparticles in the combustion aerosol process. c, [26].

We observed an increase in the lattice constant at the level of 0.5 % for A1C, A2 and A2C/PVP samples and at the level of 0.09 % for sample A3C, compared with the data for spinel from the database a = 8.0848 Å. This increase is related to the extension of the crystal lattice of the spinel resulting from the presence of rare earths ions, where ionic radii amounts to Er^{3+} (0.103 nm) and Yb^{3+} (0.1 nm), and are larger than the ionic radii of Al^{3+} (0.053 nm) and Zn^{2+} (0.0074 nm). Similar behaviour was reported by Barros *et al.* [23] in the case of Eu^{3+} doped $ZnAl_2O_4$ spinel obtained by combustion reaction. In this case, the increase was at 0.02 %. By using the Scherrer's equation [32] the average size of the crystallite grains was determined from all the reflections to be ca. 11 nm to 21 nm. In each of analyzed samples we observed strongest five peaks characteristic of the $ZnAl_2O_4$ spinel (Table S1 in Supporting Information).

TEM images of the $ZnAl_2O_4$ doped with Er^{3+} and Yb^{3+} calcined at 990 ºC for 3 hours and PVP coated nanoparticles are shown in Fig. 3. Fig. 3a, e depicted typical TEM images of $ZnAl_2O_4$ nanoparticles doped Er^{3+} and Yb^{3+} and diffraction contrast performed using bright field technique for selected samples, respectively. Fig. 3b, f and j showed TEM images of these nanoparticles in dark-field view. Spheres are constructed with primary nanoparticles (ca. 11 nm to 21 nm). [19] HRTEM image revealed the atomic structure of the spinel crystallites (Fig. 3c, g, k). We observed a useful for bioimaging size distribution of nanoparticles for all the samples tested. A comparison of nanoparticles diameter histograms (for the 4 M sample) is presented in Fig. 3d and h. The particles obtained from an

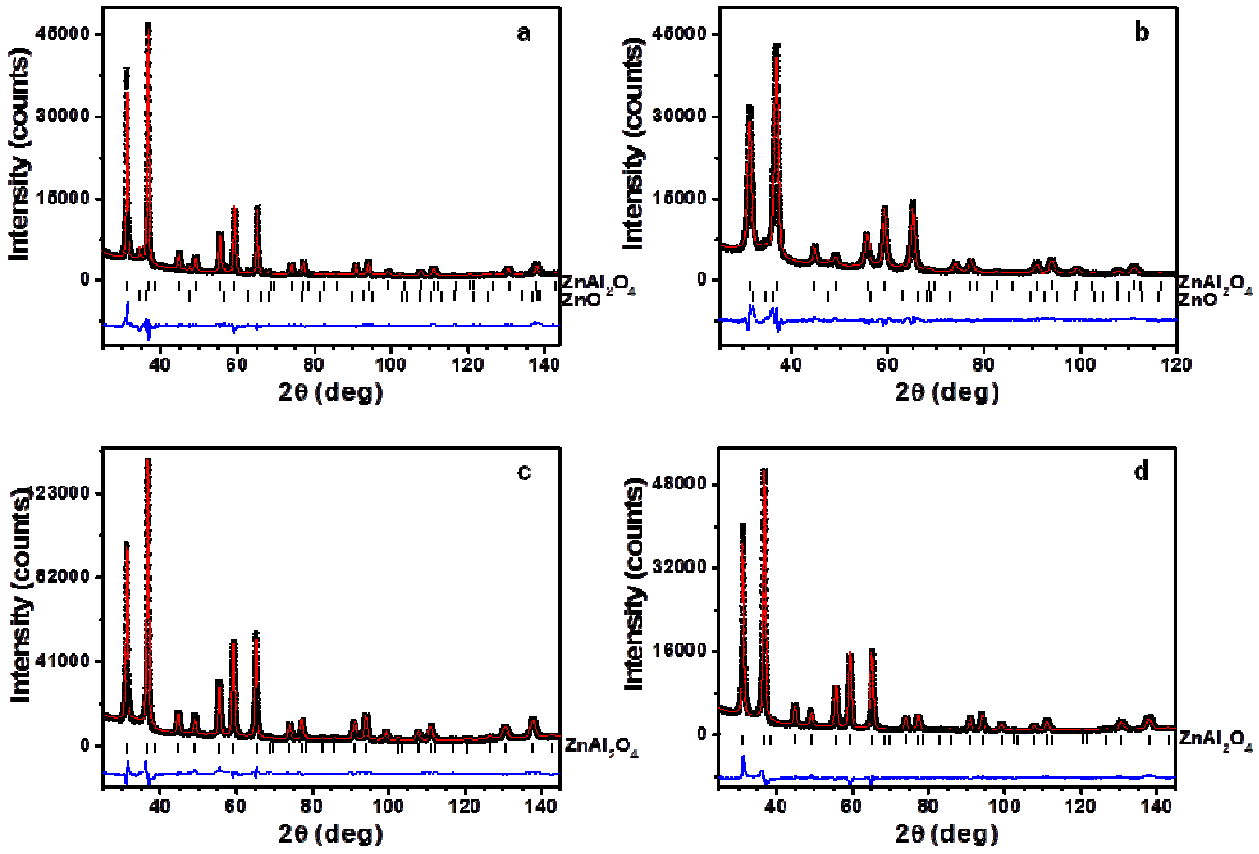

Fig. 2 Rietveld refinement for the spinel type ZnAl1.9Er0.017Yb 0.083O4 nanocrystalline powder. The two samples are present reflections originating from ZnO. A1 sample calcined at 990 ºC for 3h. a, A2 sample not calcined. b, A2C/PVP sample calcined at 990 ºC for 3h, then coated with a PVP. c, A3C sample calcined at 990 ºC for 3 h. d, Ordered with the dilution level. Points represent the pattern. The curves represent the pattern calculated theoretically. The blue marked differential curves.

aqueous solution, without ethanol (Fig. 3d, sample A1C/PVP), have a broader size distribution and greater particle diameter (d = 136 nm), than particles obtaining from a solution of ethanol-enriched in the starting solution (Fig. 3 h, sample A2C/PVP), d = 82 nm. The addition of ethanol resulted in an increase in the temperature of the process and lowering of droplets sizes obtained from the nebulizer. Fig. 3l shows the size distribution of the particles corresponding to the TEM micrographs in Fig. 3i, j, k for A3C/PVP sample, d = 140 nm. Fig. S1 in Supporting Informations summarized the Scanning Electron Microscope (SEM) images. They revealed morphological changes in the surface of the $ZnAl_{1.9}Er_{0.017}Yb_{0.083}O_4$ spinel nanoparticles and depicted topographies of the nanoparticles surface. The average particle size and the size distribution were determined using Zeiss Smart Tiff program. Table S2 in Supporting Information, compared the results obtained by both techniques. Additionally, Energy Dispersive X-ray analysis (EDX) was performed to establish distribution of elements in the samples. The results (Fig.S1 h, i) confirmed the presence of all expected elements in the spinels (Zn, O, Er and Yb). The microanalysis of chemical composition was carried out for A1 samples before and after calcinations. The ratio of the donor to the acceptor in the sample was 4.26±0.08 (from 4.82 in the precursor solution); Zn^{2+}/Yb^{3+} was 11.14±0.21 (from 8.08 in the precursor solution); Zn^{2+}/Er^{3+} was 47.75±0.18 (from 38.97 in the precursor solution); Al^{3+}/Yb^{3+} was 20.33±0.13 (from 19.36 in the precursor solution); Al^{3+}/Er^{3+} was 86.73±0.10 (from 93.38 in the precursor solution); Al^{3+}/Zn^{2+} was 1.81±0.23 (from 2.39 in the precursor solution). The detailed results are provided the in Table S3 in Supporting Information. The results confirmed the quantitative content of the elements used before (substrates) and present in the reaction products. Larger nanoparticles were used to examine the elements distribution present in the samples.

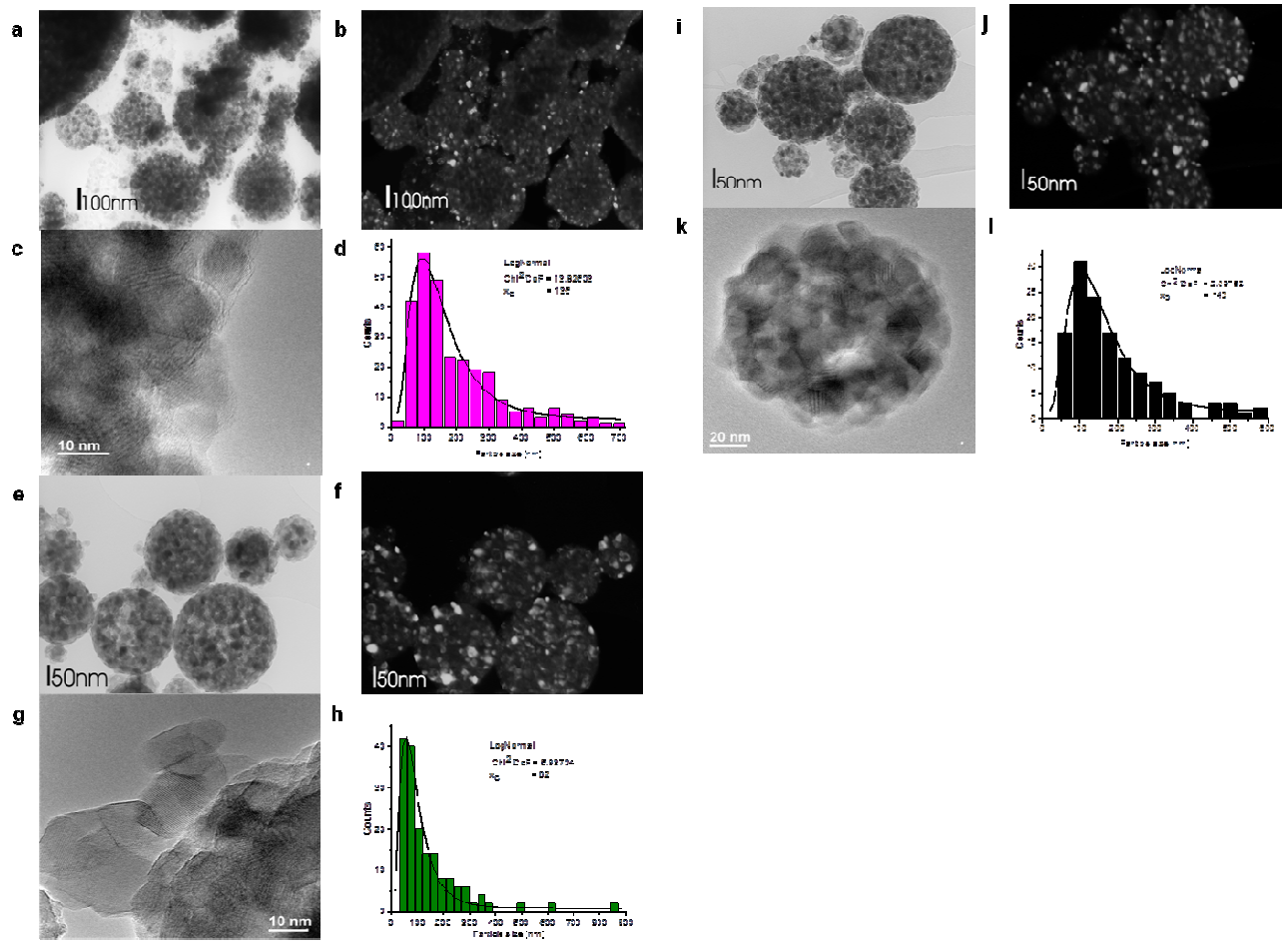

Fig. 3 Transmission electron microscopy (TEM) image of: A1 sample calcined at 990 ºC for 3 h and coated PVP, bright field. a, Dark field. b, HRTEM images for the NPs. c, Size distributions for these NPs. d, A2 sample calcined at 990 ºC for 3 h and coated PVP: bright field. e, Dark field. f, HRTEM images for the NPs. g, Size distributions for these NPs. h, A3 sample calcined at 990ºC for 3h and coated PVP: bright field. i, Dark field. j, High-magnification TEM image selected fragment. k, Size distributions for A3 sample calcined at 990 ºC for 3 h and coated PVP in l .

Cite this: DOI: 10.1039/c0xx00000x

www.rsc.org/xxxxxx

3.2 Luminescence properties

Photoluminescence of the $ZnAl_2O_4$ doped with Er^{3+} and Yb^{3+} nanoparticles was measured prior and after calcinations, and PVP coating, in the powder form, resulting from the initial solutions: A1, A2, A3, A4 and A5. Spectra were recorded at continues wave (CW) 965 nm laser diode with the power density (P_d) of 120 mW mm^{-2}, 400 mW mm^{-2} and 584 mW mm^{-2} (Fig. 4a to j). By using a molecular visualization and animation program VMD (Visual Molecular Dynamics) [33] the unit cell geometry of $ZnAl_2O_4$ spinel (Fig. 5a) was designed. Then atoms of Er^{3+} and Yb^{3+} were tossed randomly. Their number, in relation to the number of atoms modelling crystal lattice, was calculated based on the ratio Yb^{3+} to Er^{3+}. As a result we obtained animation layouts of the upconversion process (Fig. 5b). The following steps of the energy transfer between donor (Yb^{3+}) and the acceptor (Er^{3+}) are proposed as follows: 1. Infrared photons induce ytterbium atom, 2. Ytterbium atom transfers energy (ET) to the erbium atom, 3. Ytterbium atom absorbs additional infrared photons, 4. Erbium atom absorbs additional energy and releases it as a red light. The typical energy-level diagram for the upconversion luminescence from materials doped with these ions under infrared excitation is shown in Fig. 5c. The 980 nm infrared photons are absorbed by Yb^{3+} ions, and then the energy is transferred to the activator Er^{3+} ions in a two-step ET. [34] ET is one of three different classes of UC processing mechanisms which can lead to the two (or more) photon absorption. As a results, distinctive Er^{3+} emission bands at 550 (green) and 661 nm (red), were observed in each case. Followed by a multi-phonon relaxation process, Er^{3+} lost part of its energy from excited state $^4F_{7/2}$ to lower excited state $^4S_{3/2}$, then returned to ground state $^4I_{15/2}$, emitting green light. The red light predominance phenomenon could be explained by the fast non-radiative cross-relaxation process, which might result from segregation of Er^{3+} on the core [35] cluster formation of RE^{3+} ions in $ZnAl_2O_4$ host. Impurities like NO_3^-, OH^-, with high phonon energy, present on nanoparticles surface and boundary of grains, may radically increase the multiphonon relaxation from $^4S_{3/2}$ ($^2H_{11/2}$) to $^4F_{9/2}$ level. Consequently, this may result enhanced population in $^4F_{9/2}$ state, which was responsible for the red luminescence. [36, 37] Table S4 the relative number of photons determined from the PL measurements obtained at three power density (P_d) 120 mW mm^{-2}, 400 mW mm^{-2} and 584 mW mm^{-2}, for all samples tested (excitation of 965 nm). The relative number of photons emitted from each of the samples was analyzed counting the area under the emission spectrum integrating, with maxima at 661 nm and 547 nm obtained from the photoluminescence measurements. The highest ratio of the red luminescence intensity to the green luminescence (I_{red}/I_{green}) was observed for the sample A2C/PVP, with an average particle size of 133 nm, designated from the SEM measurements (Table S2). In our previous study, [18] we reported the luminescence changes for various ytterbium content in the lattice crystal and selected the optimal concentration responsible for the spinel luminescence. Comparable values were observed for the samples A3, A4 and A5 for the luminescence intensity area at 661 nm, and the power density P_d = 120 mW mm^{-2}. In the case of the the power density P_d of 584 mW mm^{-2}, the highest value of the luminescence intensity was obtained for the sample A3 (2.7 M starting solution). Upon calcination, followed by the PVP passivation, the nanoparticles luminescence intensity increased for all tested samples (Fig. 4). PVP, which is a water soluble polymer, was used as a capping polymer to stabilize the nanoparticles. [38] For comparison, for samples prepare without urea in the starting solution, the highest intensity (I_{red}) was obtained for A3C/PVP sample at 400 mW mm^{-2}.

We have selected 980 nm excitation (instead of 800 nm) to optimize the red emission in the Er-Yb system suitable for the Rose Bengal Reactive Oxygen Species (ROS) generating excitation. However, if the ROS generation capability is not desired, the 800 nm excitable upconversion could be preferred to minimize overheating issues [39].

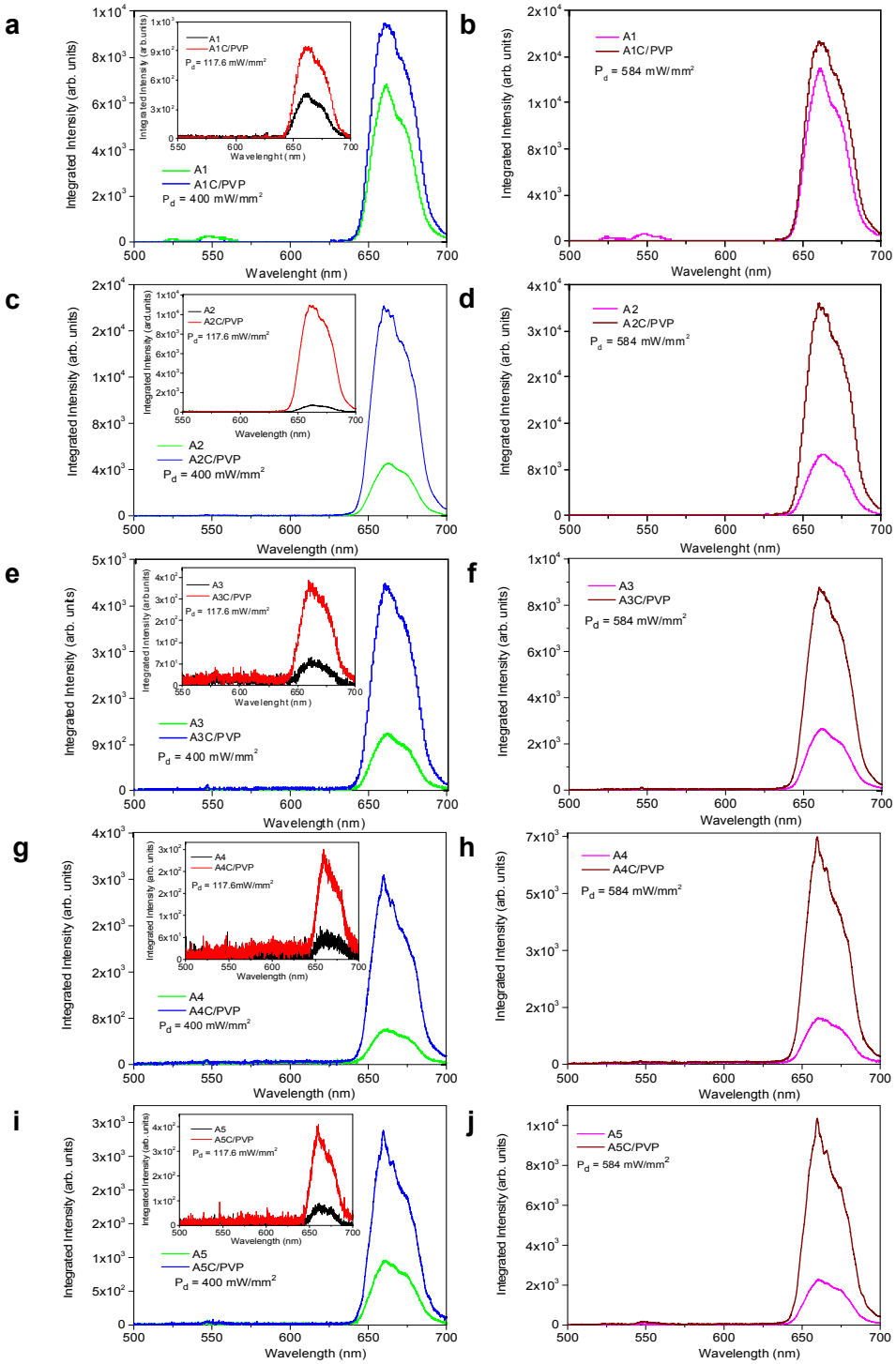

Fig. 4 Comparison of photoluminescence spectra of the upconverting $ZnAl_{1.9}Er_{0.017}Yb_{0.083}O_4$ nanoparticles (in powder form): not calcined and calcined (air, 3 hour - 990 °C) and then coated with PVP. Excitation: λ_{exc} = 965 nm. The spectra were obtained at CW power density (P_d) 120 mW mm^{-2}, 400 mW mm^{-2} and 584 mW mm^{-2}.

Cite this: DOI: 10.1039/c0xx00000x

www.rsc.org/xxxxxx

3.3 Uptake of spherical $ZnAl_2O_4:Er^{3+},Yb^{3+}$ spinels by living cells

We tested the application of nanoparticles as luminescent markers in biological materials. Non-functionalized and PVP functionalized spherical $ZnAl_2O_4:Er^{3+},Yb^{3+}$ nanoparticles were incubated with HeLa cells and found to be endocytosed by the cells (Fig. 6). Previously, we reported results on the PVP functionalized $NaYF_4$: Er^{3+},Yb^{3+} nanoparticles, introduced into HeLa cells. [18] Venkatachalam *et al.*[40] has reported bioimaging of M1 cells (macrophages) using 30-40 nm Er^{3+} doped Y_2O_3 nanoparticles. Further it was demonstrated that under the physiological conditions, Y_2O_3 nanoparticles emit UC and NIR fluorescence in M1 cells even after the surface modification with PEG-b-PAAc polymer. Hemmer *et al.* [41] reported the synthesis of bare and poly(ethylene glycol)-b-poly(acrylic acid) (PEG-b-PAAc) modified $Gd_2O_3:Er^{3+},Yb^{3+}$ nanostructures and the study of the cytotoxicity by incubation with B-cell hybridomas and macrophages, in vivo. Suárez-Franco *et al.*[42] investigated the effect of the surface morphology of thin films of $ZnAl_2O_4$ prepared by spray pyrolysis and bulk pellets of polycrystalline $ZnAl_2O_4$ prepared by chemical co-precipitation reaction on the cell adhesion, viability, and cell-material interactions of osteoblastic cells.

Unlike the previous work, we synthesized spherical $ZnAl_2O_4$ nanoparticles Er^{3+} and Yb^{3+} doped using combustion aerosol method and for the first time used them as a intracellular luminescent markers in cancer cells. The cells were incubated with four selected samples of $ZnAl_2O_4:Er^{3+},Yb^{3+}$ nanoparticles (2 μM): A2C/PVP , A3C/PVP and 20 μM A5C/PVP and A5 without PVP for 24 h at 37 °C and 5 % CO_2 with Lipofectamine 2000 (Fig. 6a, b, c, d). We applied the transfection agent to facilitate the $NaYF_4$: Er^{3+}, Yb^{3+} nanoparticle endocytosis. [18] After excitation by a femtosecond pulse of NIR radiation (λ = 980 nm), using a multiphoton confocal fluorescent microscope, we observed a strong luminescence resulting from the presence of intracellularly located nanoparticles. One should note the characteristic for the UC luminescence (green: 500-575 nm and red 625-700 nm). Autofluorescence from the cells was shown as green pseudocolor (the CW excited at 488 nm and detected at 508-585 nm). No biological toxicity of $ZnAl_2O_4$ oxide materials doped with Er^{3+} and Yb^{3+} has been observed on the *Caenorhabditis elegans* model (data not shown).

Significant amounts of the nanoparticles were observed inside the cells after 12 hours incubation with 2μM A2C/PVP in the presence of the liposomes (Lipofectamine) with HeLa cells. The quantity of the internalized nanoparticles further increased after 24 hours incubation with 20μM nanoparticle solution. The nanoparticles accumulated mainly in the cytoplasm, near the nucleus. The results confirmed our previous observation with the $NaYF_4:Er^{3+},Yb^{3+}$ endocytosis facilitated by the liposomes.[18]

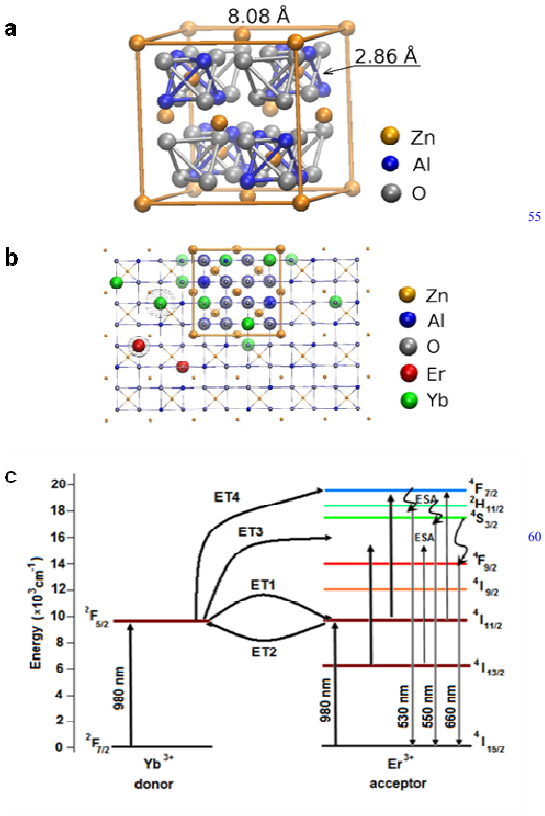

Fig. 5 The geometry of the unit cell of $ZnAl_2O_4$. a, The unit cell are marked in yellow. Aluminum atoms are marked in blue and oxygen atoms in gray. Erbium atoms (of red color) and ytterbium atoms (of green color) are randomly spread out throughout the sample. Spinel $ZnAl_2O_4:Er^{3+},Yb^{3+}$ unit cell geometry (upconversion process). b, Diagram of energy levels in the upconversion process. c

4. Conclusion

Upconverting, PVP functionalized, and non-functionalized, spherical $ZnAl_2O_4$: Er^{3+},Yb^{3+} nanoparticles (d = 80-140 nm) were synthesized by a combustion aerosol process. The method produced spinel type host $ZnAl_2O_4$ containing optimal Er^{3+} and Yb^{3+} required for an efficient upconversion of NIR excitation (high tissue penetration, low autofluorescence, minimal photodamage to red (mainly) and green emissions. The optimized red luminescence improves the signal-to-noise ratio of the nanoparticle biolabeled samples. Using the reported method, several problems mentioned above associated with applying conventional fluorophosphors for bioimaging can be avoided.

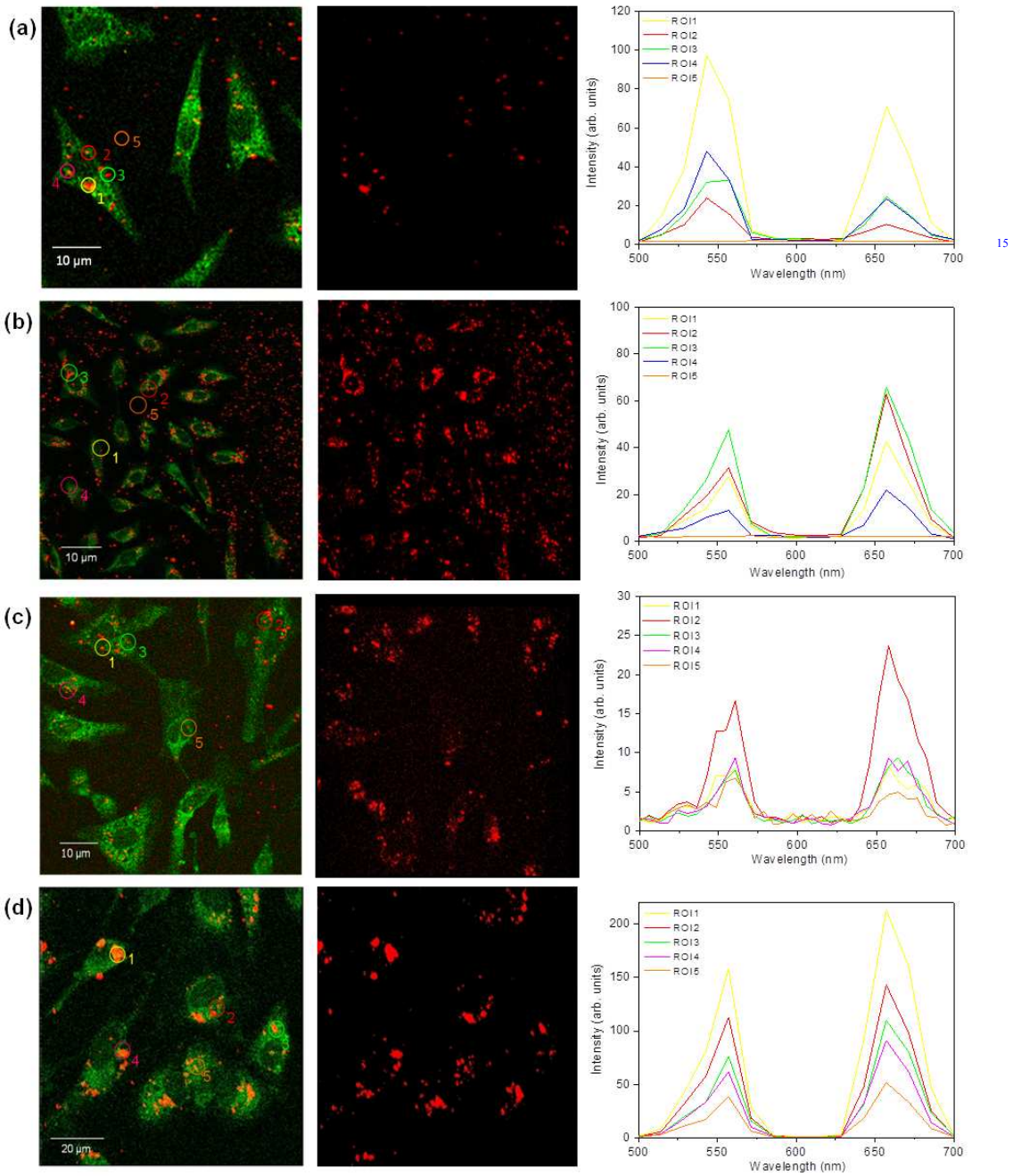

Fig. 6 Confocal images of HeLa cells after 24 h incubation in a solution of: 2µM $ZnAl_2O_4$: Er^{3+},Yb^{3+} samples a) A2C/PVP and 24 h incubation in a solution of 20µM $ZnAl_2O_4$:Er^{3+}, Yb^{3+} samples b) A3C/PVP c) A5C/PVP and d) A5C without PVP nanoparticles with Lipofectamine 2000. Autofluorescence from the cells is shown as green pseudocolor (excitation at 488 nm (CW); detection at 508-585 nm). Nanoparticles $ZnAl_2O_4$: Er^{3+}, Yb^{3+} are shown as red color with excitation at 980 nm (femtosecond laser) and detection at 500-700 nm. Inset: nanoparticle canal and the up-conversion spectra of the nanoparticles. Images obtained from confocal microscopy.

Acknowledgements

The research was partially supported by the European Union within European Regional Development Fund, through grant Innovative Economy (POIG.01.01.02 - 00 - 008/08) and was partially supported by the grant from the Polish National Science Center NN 302 663 940 and partially supported by the grant DEC-2012/07/B/ST5/02080 of the National Science Center of Poland and Center of Excellence. This work has been done in the NanoFun laboratories co-financed by the European Regional Development Fund within the Innovation Economy Operational Program, the Project No. POIG.02.02.00-00-025/09/. This research has been co-financed with the European Union funds by the European Social Fund. Acknowledgements to Prof. Grzegorz Wilczyński (Nencki Institute of Experimental Biology, Polish Academy of Science), Dr. Jakub Włodarczyk (Nencki Institute of Experimental Biology, PAS) for providing access to confocal microscopy.

Notes and references

[a] *Institute of Physics, Polish Academy of Sciences, al. Lotników 32/46, 02-668 Warsaw, Poland. Fax:(+48 22) 843 09 26 ;Tel: (+48 22) 843 66 01; E-mail: ikaminska@ifpan.edu.pl*
[b] *Institute of Genetics and Biotechnology, Faculty of Biology, University of Warsaw, ul. Pawińskiego 5a, 02-106 Warsaw, Poland*
[c] *Institute of Biochemistry and Biophysics PAS, ul. Pawińskiego 5a, 02-106 Warsaw, Poland*

1 V. Singh, R.P.S. Chakradhar, J. L. Rao and D. K. Kim, *J. Lumin.*, 2008, **128**, 394–402.
2 S. K. Sampath and J. F. Cordaro, *J. Am. Ceram. Soc.*, 1998, **81**, 649–54.
3 S. F. Wang, F. Gu, M. K. Lü, X. F. Cheng, W. G. Zou, G. J. Zhou, S. M. Wang, Y. Y. Zhou, *J. Alloys. Compd.*, 2005, **394**, 255–258.
4 R. Roesky, J. Weiguny, H. Bestgen and U. Dingerdissen, *Appl. Catal. A:Gen.*, 1999, **176**, 213-220.
5 I. Futoshi, G. Naoyuki and M. Masashi, US Pat., 5 561 089, 1996.
6 W. Strek, P. Deren, E. Lukowiak, B. Nissen, J. Wrzyszcz, M. Zawadzki and P. Pershukevich, *Spectrochim. Acta A*, 1998, **54**, 2121–2124.
7 D. L. Wood, G. F. Imbusch, R. M. Macfarlane and P. Kisliuk, D. M. Larkin, *J. Chem. Phys.*, 1968, **48**, 5255–5263.
8 H. S. C. O'Neill and W. A. Dollase, *Phys. Chem. Miner.,* 1994, **20**, 541–555.
9 A. J. Milliez, Ph.D. Thesis, Université Louis Pasteur, Strasbourg, 43, 2006.
10 F. Wang and X. Liu, *Chem. Soc. Rev.*, 2009, **38**, 4, pp. 976-989.
11 J. S. Chivian, W. E. Case and D. D. Eden, *App. Phys. Lett.*, 1979, **35**, 2, 124–125.
12 F. Wang, R. Deng, J. Wang, Q. Wang, Y. Han, H. Zhu, X. Chen and X. Liu, *Nature Material,* 2011, **10**, 968–973.
13 F. Auzel, *Chem. Rev.*, 2004, **104**, 139–173.
14 I. Etchart, Ph.D. Thesis, Corpus Christi College, Cambridge, 31, 2010.
15 J. Hampl, M. Hall, N. A. Mufti, Y. M. M. Yao, D. B. MacQueen, W. H. Wright and D. E. Cooper, *Anal. Biochem.*, 2001, **288**, 176–187.
16 R. S. Niedbala, H. Feindt, K. Kardos, T. Vail, J. Burton, B. Bielska, S. Li, D. Milunic, P. Bourdelle and R. Vallejo, *Anal. Biochem.*, 2001, **293**, 22–30.
17 H. J. M. A. A. Zijlmans, J. Bonnet, J. Burton, K. Kardos, T. Vail, R. S. Niedbala and H. J. Tanke, *Anal. Biochem.* 1999, **267**, 33–36.
18 B. Sikora, K. Fronc, I. Kamińska, K. Koper, S. Szewczyk, B. Paterczyk, T. Wojciechowski, K. Sobczak, R. Minikayev, W. Paszkowicz, P. Stępień and D. Elbaum, *Nanotechnology*, 2013, **24** 235702 (11pp).
19 A. S. S. de Camargo, L. A. O. Nunes, J. F. Silva, A. C. F. M. Costa, B. S. Barros, J. E. C. Silva, G. F. de Sa and S. Alves Jr, *J. Phys.: Condens. Matter*, 2007, **19**, 246209 (7pp).
20 S. E. Pratsinis, *Prog. Energy Combust. Sci.*, 1998, **24**, 197–219.
21 H. K. Kammler, L. Mädler and S. E. Pratsinis, *Chem. Eng. Technol.*, 2001, **24**, 583–596.
22 X. Y. Chen and Ch. Ma, *Optical Materials* 2010, **32**, 415–421.
23 B. S. Barros, P. S. Melo, R. H. G. A. Kiminami, A. C. F. M. Costa, G. F. de Sa and S. Alves, *J. Mater. Sci.*, 2006, **41**, 4744–4748.
24 S. R. Jain, K. C. Adiga and P. V. Verneker, *Combust. Flam.,* 1981, **40**, 71–79.
25 R. W. Siegel, *Nanophase materials: synthesis, structure, and properties*, ed. F. E. Fujita, Springer Series in Materials Science, Springer, Berlin 1994, 27, pp. 66–105.
26 M. R. Zachariah and M. J. Carrier, *J. Aerosol Sci.*, 1999, **30**, 9, 1139–1151.
27 P. Kumbhakar, D. Singh, C. S. Tiwary and A. K. Mitra, *Chalco. Lett.,* 2008, **5**, 12, 387–394.
28 Powder Diffraction File Card No. 5-669, International Centre for Diffraction Data, Newtown Square, PA, 1990.
29 H. M. Rietveld, *J. Appl. Cryst.*, 1969, **2**, 65-71.
30 L. B. McCusker, R. B. Von Dreele, D. E. Cox, D. Louër and P. Scardi, *J. Appl. Cryst.* 1999, **32**, 36-50.
31 T. Roisnel and J. Rodriguez-Carvajal, *Mater. Sci. Forum*, 2001, **118**, 378–381.
32 P. Klug and L. E. Alexander, *X-ray Diffraction Procedure*, Wiley, New York, 2nd edn., 1954, pp. 992.
33 W. Humphrey, A. Dalke and K. Schulten, *VMD - Visual Molecular Dynamics*, *J. Molecular Graphics,* 1996, **14**, 33-38.
34 A. M. Pires, O. Antonio Serra, S. Heer and H. U. Güdel, *J. App. Phys.*, 2005, **98**, 063529.
35 D. Yuan, G. S. Yi and G. M. Chow, *J. Mat. Res.*, 2009, **24**, 2042–2050.

36 I. Hyppänen, J. Hölsä, J. Kankare, M. Lastusaari and L. Pihlgren, Hindawi Publishing Corporation *J Nanomat.*, 2007, **5**, 1–8.
37 A. C. F. M. Costa, R. H. G. A. Kiminami, P. T. A. Santo and J. F. Silva, *J. Mater. Sci.,* 2013, **48**, 172-177.
38 W. Wu, X. Zou, Q. Li, B. Liu, B. Liu, R. Liu, D. Liu, Z. Li, W. Cui, Z. Liu, D. Li, T. Cui and G. Zou, *J. Nanomat.,* 2011, 841701, 1–5.
39 X. Li, R. Wang, F. Zhang, L. Zhou, D. Shen, Ch. Yao, D. Zhao, *Scientific Reports*, 2013, 3 : 3536, 1–7, DOI: 10.1038/srep03536.
40 N. Venkatachalam, Y. Okumura, K. Soga, R. Fukuda and T. Tsuji, *J. Phys.: Conf. Ser.,* 2009, **191**, 012002.
41 E. Hemmer, T. Yamanao, H. Kishimoto and K. Soga, *Acta Biomaterialia*, 2013, **9**, 4734–4743.
42 J. L. Suárez-Franco, M. García-Hipólito, M. Á. Surárez-Rosales, J. A. Fernández-Pedrero, O. Álvarez-Fregoso, J. A. Juárez-Islas, , M. A. Álvarez-Pérez, Hindawi Publishing Corporation, *J Nanomat.,* 2013*,* 361249*,* 1-7.